https://doi.org/10.5194/acp-2019-511
Preprint. Discussion started: 6 June 2019

Atmospheric Chemistry and Physics Discussions

Size-dependent ice nucleation by airborne particles during dust events in the Eastern Mediterranean

Naama Reicher[1], Carsten Budke[2], Lukas Eickhoff[2], Shira Raveh-Rubin[1], Ifat Kaplan-Ashiri[3], Thomas Koop[2] and Yinon Rudich[1]*

[1] Department of Earth and Planetary Sciences, Weizmann Institute of Science, 76100 Rehovot, Israel
[2] Faculty of Chemistry, Bielefeld University, Universitätsstraße 25, 33615 Bielefeld, Germany
[3]Chemical Research Support, The Weizmann Institute of Science, 76100 Rehovot, Israel

Correspondence to: Yinon Rudich (yinon.rudich@weizmann.ac.il)

Abstract. Predictions of cloud ice formation in climate models remain a challenge, partly due to the complexity of ice-related processes. Mineral dust is a prominent aerosol in the troposphere and is known to be an important contributor to ice nucleation in mixed phase clouds, as dust can initiate ice heterogeneously at relatively low supercooling conditions. We characterized the ice nucleation properties of size-segregated mineral dust sampled during dust events in the Eastern Mediterranean. The sampling site allowed us to compare between the properties of airborne dust from several sources with diverse mineralogy that passed over different atmospheric paths. We focused on particles with six size-classes, determined by the Micro-Orifice Uniform Deposit Impactor (MOUDI) cut-off sizes: 5.6, 3.2, 1.8, 1.0, 0.6 and 0.3 µm. Ice nucleation experiments were conducted in the WeIzmann Supercooled Droplets Observation on Microarray (WISDOM) setup, where the particles are immersed in nanoliter droplets using a microfluidics technique. We observed that the activity of airborne particles depended on their size-class, where supermicron and submicron particles had different activities, possibly due to different composition. The concentrations of ice nucleating particles and the density of active sites (ns) increased with the particle size and particle concentration. The supermicron particles in different dust events showed similar activity, which may indicate that freezing was dominated by common mineralogical components. Combining recent data of airborne mineral dust, we show that current predictions, which are based on natural dust or standard mineral dust, overestimate the activity of airborne dust, especially for the submicron class, and therefore we suggest to include information of particle size in order to increase the accuracy of ice formation and, thus, weather and climate predictions.

1 Introduction

Cloud droplets can supercool to 238 K before homogeneous freezing occurs (Koop and Murray, 2016; Rosenfeld and Woodley, 2000). At warmer temperatures, the common pathway of ice formation is heterogeneous ice nucleation (HIN), where the presence of aerosol particles lowers the required energy barrier to form a stable ice nucleus (Hoose and Möhler, 2012;

https://doi.org/10.5194/acp-2019-511
Preprint. Discussion started: 6 June 2019


Atmospheric Chemistry and Physics Discussions

Khvorostyanov and Curry, 2004; Murray et al., 2012; Pruppacher and Klett, 1997). These ice-nucleating particles (INPs) can be activated at various sub-zero temperatures and subsequently lower humidity conditions, mainly by interaction with supercooled droplets. INPs are relatively rare particles and comprise only about 10^{-5} of the total ambient particles in the free troposphere. Yet, their interaction with clouds can greatly influence climate. Therefore it is important to represent them well in weather and climate models (DeMott et al., 2010). Currently, ice formation is a source of great uncertainty in cloud and climate models, partly due to the complexity of ice processes and the insufficient understanding of the key properties which determine an INP (IPCC, 2013). To improve the predictions of models, a great effort is invested in characterization of INPs and in the development of parametrizations based on their physical and chemical properties (Cantrell and Heymsfield, 2005; Niemand et al., 2012; Ullrich et al., 2017).

One of the most prominent INP in the atmosphere is mineral dust, which originates in dryland zones, such as deserts (DeMott et al., 2003; Middleton, 2017). Mineral dust has high spatial and temporal variability, impacting atmospheric, oceanic, biological, terrestrial and human systems (Garrison et al., 2003; Gat et al., 2017; Jickells et al., 2005; Mahowald et al., 2014; Mazar et al., 2016; Middleton and Goudie, 2001). Each year gigatones of dust are transported globally over long distances, dominating the atmospheric aerosol mass and aerosol optical depth (AOD) (Ben-Ami et al., 2010; Chiapello et al., 1999; Koren et al., 2006; Prospero, 1999; Tegen and Fung, 1994). Field observations have identified an increase in INP concentrations and ice clouds formation in the presence of mineral dust (Ansmann et al., 2008; Rosenfeld et al., 2001). Ice residuals often contain mineral particles (Cziczo and Froyd, 2014; Cziczo et al., 2013; Twohy and Poellot, 2005). Though the exact property of an aerosol that determines its ice nucleation ability is not known, it was consistently shown that the mineral composition plays an important role (Kanji et al., 2017). Mineral dust samples are often chemically similar but differ in their mineralogy (Engelbrecht et al., 2009), and the particles are often composed of a mixture of minerals (internally mixed), such as clays, quartz, feldspars and calcites. Other common minerals are palygorskite, hematite, halite, gypsum, gibbsite and goethite (Ganor et al., 1991; Kandler et al., 2007; Mahowald et al., 2014; Perlwitz et al., 2015). The mineralogy of mineral dust is set by its source region and is considered to be an important factor that determines its freezing characteristics (Augustin-Bauditz et al., 2014; Zimmermann et al., 2008). Using standard mineral particles, Atkinson et al. (2013) found that K-feldspar is a most efficient type, and suggested its importance for atmospheric ice formation above 258 K. This was further supported by measurements of natural dust from desert surfaces worldwide, where the importance of quartz mineral phases was also indicated (Boose et al., 2016b).

Airborne mineral dust (AMD) can experience chemical and physical modifications during its atmospheric transport, such as size and mineralogy differentiation or formation of coatings by sulphate, organic or biological components. These modifications, or aging processes, can alter dust's ability to nucleate ice (Hoose et al., 2008; Kanji et al., 2017; Laskin et al., 2005; Möhler et al., 2008; Murray et al., 2012; Sullivan et al., 2010). While there are only few measurements of AMD near source regions (Price et al., 2018), parameterizations of ice formation in climate models are often based on the freezing properties of surface-sampled natural dust samples (Niemand et al., 2012), that may not be sufficiently representative for AMD. Natural dust samples showed higher ice nucleation ability than AMD samples, possibly because of the atmospheric

https://doi.org/10.5194/acp-2019-511
Preprint. Discussion started: 6 June 2019


Atmospheric Chemistry and Physics Discussions

processing of AMD that lead to deactivation, and possibly due to laboratory processes, which were applied to the natural dust samples, and may have enhanced its activity (Boose et al., 2016b).

In this study, we investigated airborne particles sampled in Israel during six events of high AMD loadings. The Eastern Mediterranean is located in the strip of the world's main deserts, and is often affected by dust storms from several sources: (i) dust from the Saharan Desert, initiated in North Africa, and transported over North Africa and/or the Mediterranean Sea, or (ii) dusts from the Syrian and the Arabia deserts east and south-east of Israel, and transported over land (Ganor et al., 1991). These distinct sources and paths allow investigating the ice nucleation properties of AMD with diverse origins and transport paths. The collected particles were size-segregated using the Micro-Orifice Uniform Deposit Impactor (MOUDI), and their ability to initiate immersion freezing was investigated. Ice nucleation experiments were performed with the Weizmann Supercooled Droplets Observation on a Microarray (WISDOM) instrument which employs nanoliter droplets (Reicher et al., 2018). One of the events was sampled and studied also in the Bielefeld Ice Nucleation ARraY (BINARY) (Budke and Koop, 2015), which employs microliter volumes. The use of droplets with larger volumes increases our sensitivity to detect nucleation sites that are relatively rare. In this study, we characterize the concentrations and the density of ice nucleation active sites (INAS) of AMD in different size-classes for diverse dust cases, as well as combine recent literature and available AMD data to understand how well AMD is represented in climate models based on recent parameterizations.

2 Data and Methods

2.1 Sampling

Airborne particles were sampled during six high dust events in 2016 and 2017, detailed in Table 1. Sampling started when the visibility was reduced due to increasing concentrations of particulate matter (PM). The sampling site was located on a roof of a three-story building in Rehovot, Israel (31.9N, 34.8E about 80m AMSL). The location is often impacted by mineral dust storms, transported from nearby and distant geographical locations, mainly from the Sahara and Arabia deserts, and less frequently from the Syrian Desert, depending on the season and the synoptic conditions (Dayan, 1986; Ganor et al., 2010; Kalderon-Asael et al., 2009).

Particles were collected on polycarbonate filters (47mm cyclopore, 0.1 μm isopores; Whatmann), using the MOUDI impactor (model 110-R), a 10-stage impactor with 18 μm cut-point inlet stage followed by size segregating stages with cut points (D_{50}) between 0.056 and 10 μm in aerodynamic diameter (Marple et al., 1991). Sampling time ranged between 17 and 48 h with a 30 L min^{-1} sample flow rate, similarly to previous studies (Huffman et al., 2013; Mason et al., 2015).

2.2 Air mass Back Trajectories

Back trajectories were calculated by a Lagrangian method, using LAGRANTO 2.0 (Sprenger and Wernli, 2015). The calculation of air mass trajectories was based on wind data from the European Centre for Medium-Range Weather Forecasts ERA-Interim reanalysis (Dee et al., 2011), available every 6 h, at 1°×1° horizontal grid and 60 vertical hybrid levels. For each

https://doi.org/10.5194/acp-2019-511
Preprint. Discussion started: 6 June 2019


Atmospheric Chemistry and Physics Discussions

6-h time step within the duration of each event, trajectories were calculated 72 h backward from the sampling site, from all available data grid points with pressure larger than 850 hPa, resulting in 11 trajectories, which end their path in the lower troposphere for each calculation. In a second step, the Eulerian densities of the resulting trajectories were computed by gridding the trajectories for each event, smoothed by using a radius of 100 km and interpolated to 1 h. Finally, the trajectory density was summed over the entire event duration and normalized by the maximum trajectory count.

2.3 Dust Column Mass Density Maps

Time averaged maps of dust column mass density (hourly 0.5°×0.625°) reanalysis data were obtained from the Modern-Era Retrospective analysis for Research and Applications (MERRA-2). Maps were produced using NASA's Global Modeling and Assimilation Office (GMAO) (Gelaro et al., 2017), for a period of up to 72 h prior to the sampled event.

2.4 Particulate Matter Data

Particulate matter mass data were obtained from the Israeli Ministry of Environment website. Concentrations of particles with aerodynamic diameters smaller than 10 µm (PM_{10}) were measured in the Rehovot station, located close to our sampling site. The 5-minutes mean data was used to calculate peak and mean concentrations of the sampled dust events.

2.5 Particle Number-Size and Surface Area distributions

Characterization of particle size distribution and concentrations was based on optical particle counter measurements between 0.25 and 32 µm (OPC; GRIMM Technologies model 1.109), conducted in parallel to the MOUDI sampling. Estimation of particle surface area assumed sphericity and diameter was taken as the midpoint of the GRIMM's channels.

2.6 Conversion of GRIMM channels to MOUDI stages

To determine the total surface area collected on MOUDI's filter, a conversion matrix between the GRIMM channels and the MOUDI stages was applied. The conversion was based on the particle collection efficiency curves of the MOUDI and inter-stage particle losses reported in Marple et al. (1991). Figure 1 demonstrates the fraction of particles that are collected on the stages based on their aerodynamic diameter. The detailed stages, stage #2 (D_{50} = 5.6 µm), stage #3 (D_{50} = 3.2 µm), stage #4 (D_{50} = 1.8 µm), stage #5 (D_{50} = 1.0 µm), stage #6 (D_{50} = 0.6 µm) and stage #7 (D_{50} = 0.3 µm), are the stages that freezing analysis was focused on. For example, most of the particles with an optical diameter > 8.5 µm will be collected on stage #2 (D_{50}=5.6 µm), whereas all the particles with an optical diameter > 17.5 µm are assumed to be collected on former stages (inlet and stage #1). In some cases, particles in a certain size are likely to impact on two different MOUDI stages. For example, a small fraction of 0.5 µm particles are impacted on stage #5 (D_{50}=0.6 µm), and most of them impact on stage #6 (D_{50}=0.3 µm). The initial particle concentration that was used is the accumulated sum of all particles for the entire sampling period.

https://doi.org/10.5194/acp-2019-511
Preprint. Discussion started: 6 June 2019

Atmospheric Chemistry and Physics Discussions

2.7 Ice Freezing Experiments and Quantification

2.7.1 WISDOM

Immersion freezing properties were measured using suspensions of the collected dust particles that were extracted from the filters using sonication (VialTweeter, model UP200St; Hielcher). A quarter filter was inserted into a 1.5 ml Eppendorf vial with 0.3 ml deionized water, and sonicated in three 30 sec cycles, to avoid heating. The suspension was immediately used for droplet production and freezing experiments in WISDOM as detailed in Reicher et al. (2018). Briefly, an array of 0.5 nL monodispersed droplets (~100 μm diameter, suspended in an oil mixture) was generated in a microfluidic device that was cooled by a commercial cooling stage (THMS600, Linkam) under a microscope (BX-51 with 10X magnification, Olympus) coupled to a CCD camera. The device was first cooled at a faster constant rate of 10 K min-1 from room temperature to 263 K, and then using 1 K min-1 constant cooling rate until all the droplets were frozen. The temperature uncertainty was ± 0.3 K, based on error propagation between the calibrated droplet temperature and the uncertainty of the temperature sensor, that is located in the cooling stage (see Reicher et al. (2018) for more details).

2.7.2 BINARY

The Bielefeld Ice Nucleation ARraY (BINARY) is an optical freezing array of droplets pipetted on a hydrophobic substrate in separated sealed compartments and cooled in a Linkam cooling stage (LTS120) (Budke and Koop, 2015). In the present study an array of 64 droplets of 0.6 μL was employed. Suspensions were prepared by extracting a quarter filter in 1.5 ml of double-distilled water (that is, 5 times more diluted than WISDOM suspensions), using a bath sonicator (Elma Transsonic Digital (TP 670/H)) for 30 min. The bath temperature increased during sonication from about 288 to 308 K. The obtained suspensions were used directly and further diluted (1:10) for another set of measurements with reduced surface area of the particles in the droplets. For the freezing experiments, the droplets were cooled at 1 K min^{-1}. Temperature uncertainty was ±0.3 K.

2.7.3 Quantification of Freezing Properties

The cumulative concentration of ice nuclei present in a volume of solvent, V, at temperature, T, was derived using the fraction of frozen droplets ($f_{ice}(T)$), that was obtained directly from the freezing experiments (Vali, 1971):

$$K(T) = \frac{-ln(1-f_{ice}(T))}{V} \quad [cm^{-3}\ of\ water] \qquad (1).$$

For control experiments, a quarter of blank filter was immersed in pure water, similarly as was done in the freezing experiments of the airborne samples, and the concentration of the background impurities ($K_{\mathrm{imp}}(T)$) were subtracted from the concentrations that were detected for airborne samples.

The atmospheric concentrations of INP per unit volume of air as a function of temperature, $INP(T)$, were determined for the airborne samples by incorporating the sampling and solvent parameters into Eq. 2 (Hader et al., 2014):

$$INP(T) = \left(K(T) - K_{imp}(T)\right)\frac{V_{\mathrm{solvent}}}{\mathrm{f}\cdot V_{\mathrm{air}}} \quad [\mathrm{cm}^{-3}\ \mathrm{air}] \qquad (2),$$

https://doi.org/10.5194/acp-2019-511
Preprint. Discussion started: 6 June 2019


Atmospheric Chemistry and Physics Discussions

where $V_{solvent}$ is the volume of extracting solvent, V_{air} is the total sampled air volume, and f is the fraction of filter that was used in the extraction (for example, $f = 0.25$ for a quarter filter).

To compare the ice nucleation activity of the different dust events, the ice nucleating particle concentration in the liquid was converted to the number of active sites per unit surface area of INPs, i.e., the surface density of sites n_s active above temperature, T (Vali, 1971):

$$n_s(T) = \frac{-ln(1-f_{ice}(T))}{A} \quad [m^{-2}] \qquad (3),$$

where A is the surface area that was immersed in a single droplet of the experiment.

2.8 Scanning Electron Microscopy

A quarter of selected filters were coated with Iridium for analysing the chemical composition of airborne particles using a scanning electron microscope (SEM; Supra 55VP, LEO) equipped with an Energy-dispersive X-ray spectroscopy (EDX) detector for elemental microanalysis. The analysis was done at a voltage of 5 kV using the Quantax software (Bruker).

3 Results and Discussion

3.1 Air mass Back Trajectories and the Origin of the Dust Storms

The density of air mass back trajectories for 72-h period prior to the sampling for all events are shown in Figure 2. The sampling site and the surrounding main deserts are shown as well. During the sampled events, the air mass trajectories were diverse. In some cases, the air masses travelled directly to the sampling site, while in other cases, they travelled longer distance. In most events, the air mass had either easterly or westerly component, and were often concentrated in the same geographical area.

The dust origins were identified based on back trajectory analysis, integrated with reanalysis data of remote sensing of atmospheric dust. We followed the dust mass concentration prior to the sampling period, as detailed in Figure S1. Locations that contained high levels of suspended dust and overlapped with the air mass trajectories were identified as the possible sources of dust. The green contours in Figure 2 represent the assigned dust origin for each sampled event based on the reanalysis data. Note that in two events, there was no overlap between the dust origin and air mass trajectories. These events will be further discussed below. Two events, denoted by SDS1 and SDS2, originated in North Sahara Desert. The source of SDS1 was near the border of Egypt and Libya, and the source of SDS2 was in Egypt, east of SDS1. The dust travelled over the Mediterranean Sea and was potentially affected by the marine environment, possibly obtaining a sea salt or anthropogenic sulfate coating (Levin et al., 1996). Two other events, denoted by SyDS1 and SyDS2, originated from the Syrian Desert, from western Iraq and southern Syria. Compared to the Saharan events, the dust mass density in the Syrian Desert events was relatively low.

https://doi.org/10.5194/acp-2019-511
Preprint. Discussion started: 6 June 2019


Atmospheric Chemistry and Physics Discussions

Another event was more complicated: the analysis indicates that there is one possible dust origin east of the sampling site in the Syrian Desert, and another one south of the sampling site in the Sahara Desert. However, the air mass trajectories did not overlap with the Saharan dust origin, but indicated that the air mass was transported from the Red Sea. Further analysis of the air mass trajectories prior to the sampling period in the Red Sea showed that both Sahara and Arabia dusts were transported to the Red Sea (see the supplementary part, Figure S2(a)). This event is therefore defined as a "mixed dust" event (MDS). Another event did not show overlap between the air mass trajectories and the dust origin. Further analysis of air mass back trajectories in the days prior to the sampling period, showed that dust was transported to the Mediterranean Sea from the region of Libya in the Sahara Desert, towards Turkey, and was deflected eastward by westerly winds to the sampling site (see the supplementary part, Figure S2(b)). The dusty air masses rapidly cleared up, and relatively non-dusty air masses arrived at the sampling site, as inferred from PM_{10} concentrations and the OPC size distributions, see section 3.2. This event was defined as "clean and Saharan dust storm" and denoted by CSDS. Table 1 summarizes the sampled events, their sampling periods, and the peak and mean PM_{10} concentrations during sampling. Peak values ranged from 67 μg m^{-3} in CSDS and 132 μg m^{-3} in SyDS1, to 717 μg m^{-3} in SDS2, which was the strongest dust event in this study. In SDS1, MDS and SyDS2, the values ranged between ~300 to 400 μg m^{-3}. When comparing the mean PM_{10} concentrations during the entire sampling periods, CSDS was categorized as a non-dusty event, with the lowest concentrations of 30±13 μg m^{-3}, i.e. below the threshold of 42 μg m^{-3} for dusty conditions (Krasnov et al., 2014). The mean values in the rest of the events ranged from 76 to 206 μg m^{-3}, and were therefore categorized as dust storms.

3.2 Particle Number-Size Distributions

Figure 3(a) describes the mean particle number-size distributions of sampled air during the dust events, as was detected by the GRIMM OPC. The lowest channel of the GRIMM includes only particles that are larger than 0.25 μm. This channel underestimates the total particle count since the counting efficiency is less than 100%.

The number-size distributions had similar patterns in all the events. The highest particle number concentrations were in the submicron size range, decreasing sharply towards larger particles. Events SDS1, SDS2, and MDS had a rather similar particle concentration distribution. Event SyDS1 showed similar particle concentrations in the submicron range, but the particle concentrations in the supermicron range were about an order of magnitude lower, which was also indicated in the PM_{10} data. CSDS, a predominantly non-dusty event, had the lowest particle concentrations in comparison to the rest of the sampled events, as was also indicated by the PM_{10} data. In the SyDS2 event, exceptionally high concentrations in the supermicron range above 3 μm were observed, and the peak extended towards larger particle sizes, combined with relatively high particle concentrations. Note that prior to and during this event, biomass burning events occurred east and north of the sampling site, and therefore, this peak may be attributed to contributions from biomass burnings particles. This is further supported by the SEM-EDX analysis of the filters from this event, which in comparison with the other events, contained super-aggregate particles, typically

https://doi.org/10.5194/acp-2019-511
Preprint. Discussion started: 6 June 2019


Atmospheric Chemistry and Physics Discussions

observed in biomass burning emissions, in the supermicron range, (Chakrabarty et al., 2014), with distinct morphologies and elemental composition (shown in the supplementary part in Figure S3).

The surface-area-size distributions in Figure 3(b) compares the contribution of supermicron and submicron particles to the available ambient surface area. Ice nucleation is initiates on the surface of the particles, and therefore, their surface area concentration is an important factor, in addition to number concentrations. Here it is clearly seen that the potential contribution of the supermicron particles may be significant when compared to the submicron particles, even though their number concentrations were up to two orders of magnitude lower.

3.3 Airborne INP Concentrations

The cumulative INP concentration spectra for the six dust events are shown in Figure 4. In each event, different particle size classes are marked by different color. Freezing was observed between 255 and 238 K, and the INP concentrations ranged from 10^{-4} to 1 cm^{-3} of air.

A particle size dependence of the freezing temperature and INP concentration was observed. Larger particles froze at warmer temperatures and contained higher number of INPs. The variation between the six size-classes ranged from 1 to 2 orders of magnitude, whereas in some cases the smallest particles had similar behavior to the large ones. For example, in event SDS2, size-classes D_{50}=0.6 µm and D_{50}=0.3 µm were less ice-active than the rest of the size-classes, while in MDS, all size classes showed similar activity. As an exception, event SyDS2 showed a weaker size dependence in comparison to the other dust events, and in some size-classes, lower INP concentrations. In comparison, in the relatively non-dusty event CSDS, the variability between the different size classes was higher, especially at lower temperatures. In Figure 5, similarly to Figure 4, INP concentrations are presented, but this time arranged according to the different size classes. The variability within each size class was relatively high and spans over 2 orders of magnitude; for example, at size class D_{50}=0.3 µm near 245 K, INP concentration ranged from about 10^{-3} to almost 1 cm^{-3} of air. It is clearly seen that INP concentrations in dusty conditions (SDS1, SDS2, MDS and SyDS1) were higher than in non-dusty conditions (CSDS) for the supermicron range, but similar in the submicron range.

3.4 Size-Dependence of Ice Active Site Density ($n_s(T)$)

Figure 6 presents the $n_s(T)$ curves for the different dust events, which span the range of 10^6 m^{-2} at 253K to 10^{11} m^{-2} at 238 K. In general, $n_s(T)$ increased with the particle size. The highest n_s values were observed in the supermicron range D_{50}=5.6 µm, followed by D_{50}=3.2, 1.8 and 1.0 µm. For the latter three classes, the activity was similar within measurement uncertainties. In the submicron range, stages D_{50}=0.6 and 0.3 µm, the $n_s(T)$ values were lower than in the supermicron range and showed higher variability between the different events, except for the MDS event, that had similar activity in the submicron and the supermicron range. While INP concentrations may generally vary due to experimental parameters, such as particle concentration in the droplet or droplet size, $n_s(T)$ should account for these differences, since it is normalized by the total

https://doi.org/10.5194/acp-2019-511
Preprint. Discussion started: 6 June 2019


Atmospheric Chemistry and Physics Discussions

surface area of particles immersed in the droplet. Therefore, the effect of particle size should diminish using the $n_s(T)$ curves, if the particles' ice-nucleation ability is indeed similar. Hence, the analysis presented in Figure 6 indicates that the supermicron particles are better INP than the submicron ones, implying they have better active sites that nucleate ice at higher temperatures. Figure 7 displays the same $n_s(T)$ curves as Figure 6, but now arranged according to the different size-classes. It is observed that in the supermicron range, all $n_s(T)$ curves from the different events merge (with the exception of SyDS2) suggesting that their freezing was dominated by a common component. While the freezing activity decreases with decreasing particle size, the shape of the curves is preserved, suggesting that the abundance of this common component decreases with particle size. One possible explanation for this observation may be mineralogy segregation, known to occur with particle size: larger particles contain more primary minerals, such as K-feldspar, whereas smaller particles contain more secondary minerals, such as clays and quartz that are common in all particle sizes (Claquin et al., 1999; Perlwitz et al., 2015). Therefore, the reduced activity in the submicron range and the higher variability between the dust events, especially at D_{50}=0.3 μm, may be attributed to a different mineralogical composition of the particles, or the lack of the important ice-inducing component. Alternatively, it is also possible that the submicron particles are mixed with other particle types, which are more common in this size range, such as urban pollution (Weijun et al., 2016), and therefore freezing may not be dominated exclusively by mineral dust. Moreover, due to their larger surface-to-volume ratio, submicron particles are more sensitive to atmospheric processing than supermicron particles, which can lead to further deactivation of their ice active sites (Boose et al., 2016a). These considerations may explain the variability in the activity between different events. For example, the passage of SDS1 and SDS2 over the Mediterranean Sea can contribute to their reduced activity in the submicron range, while for the MDS event, a shorter and relatively direct transport path resulted in less atmospheric processing, which may possibly explain why the freezing activity of submicron particles converged with those of the supermicron particles.

In Figure 7, we also compare a few relevant $n_s(T)$ curves of standard minerals, as derived by Atkinson et al. (2013) and Niedermeier et al. (2015), with our $n_s(T)$ curves. The standard curves of K-, Na/Ca-feldspar and quartz were scaled to the estimated fraction of these minerals in AMD (see Table S1), and are typically used for prediction of AMD ice nucleating activity. A good agreement of the absolute n_s values was observed in the relevant temperature range, and the slopes of the curves were similar to those of the feldspars, especially for the supermicron range. A good agreement was also observed with the standard $n_s(T)$ curve of quartz, suggesting that it contributes to freezing of the submicron particles in the lower temperature range. Note that the standard $n_s(T)$ curves of clay minerals and calcite were not plotted here despite their large abundance in AMD, because there was no overlap with the ice nucleation activity in this study. Only the freezing activity of the largest particles (D_{50}=5.6 μm) overlapped with the K-feldspar prediction of Atkinson et al. (2013), indicating that this prediction possibly overestimates the freezing activity of the entire size distribution of AMD. For the particles in the size range of $3.2 < D_{50} < 1.0$ μm, there is an overlap in activity with the K-feldspar prediction of Niedermeier et al. (2015) and Na/Ca-feldspar of Atkinson et al. (2013). However, in all cases, the feldspars predictions overestimate the freezing activity of AMD in the submicron range.

https://doi.org/10.5194/acp-2019-511
Preprint. Discussion started: 6 June 2019


Atmospheric Chemistry and Physics Discussions

The $n_s(T)$ curves of SyDS2 displays moderate slopes and lower IN activity in comparison with the other dust events, in all size classes, except for the smallest particles with D_{50}=0.3 μm. As was already mentioned, these particles were most likely mixed with smoke particles from biomass-burning events that occurred during the same period, and the filters from this event were covered with super-aggregate particles in the supermicron size, rich with potassium, similar to particles seen in other biomass burning events (Chakrabarty et al., 2014).

3.5 Comparison of WISDOM and BINARY measurements for event CSDS

A complementary analysis for the CSDS event using BINARY is shown in Figure 8. BINARY probes droplets with larger volumes and, thus, it is more sensitive to less common ice-nucleating sites that may not show a signal in WISDOM. In the BINARY experiments, two suspensions were tested, with different dilution factors, for extending our sensitivity. The higher total dust surface area per droplet sample that was investigated in the BINARY experiments, yellow markers in Figure 8, demonstrates the warmest freezing temperatures, ranging from 255 to 246 K, and the $n_s(T)$ values ranged from 10^6 to 10^9 m^{-2}. The 1:10 diluted samples (purple markers) showed freezing at lower temperatures, ranging from about 251 to 244 K, with higher $n_s(T)$ values ranging from 10^8 to 10^{11} m^{-2}. In some of the dilute cases of the BINARY experiments, the data were at the limit of the background impurities (see supplementary part, Figure S5). In order to include only data that are significantly different from the background, a criterion was set, in which only those data points that are larger by at least two standard deviations than the mean background impurities were further considered in Figure 8. If data were below that threshold, they were considered as not significant and thus were removed (e.g., the data of the D_{50}=0.6 and 0.3 μm for the diluted BINARY samples).

Figure 8 shows that there is a very good agreement between the BINARY and WISDOM data, because the $n_s(T)$ curves merged nicely into each other for each size-class. Whereas BINARY was more sensitive than WISDOM to the warmer and relatively rare active sites, WISDOM was more suited to detect the more common active sites in the low temperature range. Overall, the dependence of the freezing activity temperature range upon the surface area that was immersed per droplet is well demonstrated here, where a reduction in the surface area of the different experiments (WISDOM < BINARY diluted < BINARY) decreased the probability to observe freezing at the higher temperatures. This was also demonstrated previously in studies of standard mineral dust (Broadley et al., 2012; Marcolli et al., 2007; Reicher et al., 2018). Overall, the data shown in Figure 8 indicate the added value when using experimental techniques of different sensitivity for the purpose of measuring the concentration and active site density of INP in field studies (e.g., Atkinson et al., 2013; DeMott et al., 2016; Demott et al., 2017; Chen et al., 2018; Harrison et at., 2018).

https://doi.org/10.5194/acp-2019-511
Preprint. Discussion started: 6 June 2019


Atmospheric Chemistry and Physics Discussions

3.6 Comparison of Super- and Submicron ranges with AMD Measurements and Predictions

The particle surface area that was used to derive $n_s(T)$ represents the total airborne particles that were collected for each sample, regardless of particle composition. When mineral dust dominated the composition, as in a dust event case (see for example Figure S4 in the supplementary part), we treat $n_s(T)$ as representative for AMD freezing. Figure 9(a) compiles the $n_s(T)$ results of AMD from a few recent studies that focused on airborne particles (albeit not size-selected) during dust events. Results from our current study, excluding the events SyDS2 and CSDS that were not dominated by AMD, are presented alongside those of Price et al. (2018) and Boose et al. (2016b). Price et al. (2018) collected airborne particles in flights west of the Sahara Desert over the tropical Atlantic at altitudes of up to 3.5 km. Boose et al. (2016b) analysed airborne particles which were deposited in the Eastern Mediterranean region in Egypt, Cyprus and the Peloponnese (Greece) during dust events. Boose et al. (2016b) also sampled airborne particles during dust events over Tenerife, off West Africa.

This compilation shows that $n_s(T)$ curves from the different studies exhibit great similarities over a wide range of temperatures (236 - 265 K) for dust from different locations and geographic sources, with varying atmospheric paths and altitudes. This similarity may have significant implications for modelling ice nucleation activity by AMD, since it suggests that parameterizations can be simplified, for example by neglecting the complication of accounting for mineralogy of different geographical sources. Due to the different behaviour of submicron and supermicron particles, we also suggest that accounting for the particle size class will improve the prediction of ice clouds formation. For that purpose, we derived two basic parameterizations (Eq.4), for supermicron and submicron particles, based on the combined AMD data (including data from this study, Price et al. (2018) and Boose et al. (2016), and excluding SyDS2), which cover a wide range of temperatures, and spread more than 5 orders of magnitudes in $n_s(T)$ values. These parameterizations are the best mathematical fit for a Hill-type equation, which is normally used for fitting S-shaped data as they are observed in this compilation:

$$n_s(T) = exp[y_0 + a/(\mathrm{b} + \exp[(T - 248)/c])]\ [m^{-2}] \qquad (4)$$

where the coefficients (95% confidence bounds) for supermicron range particles are set to:

$y_0 = 11.47\ \ (10.97, 11.98), a = 24.00\ \ (22.01, 25.99), b = 1.53\ \ (1.35, 1.70), and\ c = 4.54\ \ (4.06, 5.02),$

$T \in [236K, 266K]\ \ (R - square = 0.93).$

and for submicron range:

$y0 = 9.48\ \ (8.19, 10.76), a = 23.00\ \ (20.23, 25.77), b = 1.34\ \ (1.10, 1.57), and\ c = 7.38\ \ (5.84, 8.92),$

$T \in [238K, 266K]\ (R - square = 0.93).$

Parameterizations for each individual size class can be found in Table S2 in the supplementary part.

In Figure 9(b), the parameterizations derived here are presented next to the recent parameterization of ice nucleation of desert dust by Ullrich et al. (2017). The parametrization by Ullrich et al. (2017) is based predominantly on natural surface-collected dust samples, but also contained one sample of AMD from Israel. The Ullrich et al. parameterization agrees within an order of magnitude with our supermicron data in the low-temperature range (243 - 247 K), but overpredicts $n_s(T)$ by more than an order of magnitude when compared to our submicron data and to the Price et al. (2018) data at warmer temperatures (247-259

https://doi.org/10.5194/acp-2019-511
Preprint. Discussion started: 6 June 2019


Atmospheric Chemistry and Physics Discussions

340 K). This emphasizes that AMD may not be represented correctly when based on desert dust sampled from the surface,
341 consistent with Boose et al. (2016b) who showed that the average freezing activity of AMD is reduced when compared to the
342 activity of surface desert dust. Atkinson's K-feldspar parameterization is also shown here, and as mentioned before, also
343 overpredicts the freezing activity of AMD at temperatures lower than about 255 K.

344 **4 Conclusions**

345 We characterized the INP activity of particles collected during several mineral dust events in the Eastern Mediterranean. Dust
346 from the Sahara Desert, the major source for atmospheric dust, together with dust from the Arabian and Syrian deserts were
347 included. Six size classes were studied that cover both the super– and submicron size ranges. The INP concentrations ranged
348 from 10^{-4} cm^{-3} of air in the relatively weak dust events to 1 cm^{-3} of air in the strongest event. The n_s values ranged from 10^6 to
349 10^{11} m^{-2} in the temperature range of 238 – 255 K. A size dependence was observed, both in the INP concentration and in n_s
350 values. Larger particles were more active INP, exhibited higher INP concentrations and a higher number of nucleating sites
351 per surface area at higher temperatures. Comparison between freezing results of WISDOM with BINARY showed good
352 agreement, strengthened previous studies that observed how the freezing activity could depend on technical properties and
353 limitations of the used instrumentation, and therefore emphasize the importance of using complementary instruments.
354 The dust events studied here represent a range of dust loads, different dust origins and atmospheric paths. Yet, the supermicron
355 particles in these events had similar freezing abilities. This may indicate that there is a unique component that is responsible
356 for freezing activity, as was previously suggested (Atkinson et al., 2013; Boose et al., 2016b; Kaufmann et al., 2016; Price et
357 al., 2018). Our measurements showed that the activity of the supermicron particles was in the range of standard particles of
358 feldspar mineral, and that the activity of the submicron particles was in the range of standard quartz. Therefore, we suggest
359 that these may be the two most important components that dominate the freezing by atmospheric mineral dust (AMD), and
360 therefore may be important for heterogeneous ice nucleation in atmospheric clouds. The submicron particles showed higher
361 variability between events, possibly due to different composition of the particles or higher sensitivity to atmospheric processing
362 during long-range transport.
363 Mineral dust is important both on a regional scale, near its source region, and on a global scale, since it remains ice-active even
364 after long transport in the atmosphere and thus over considerable distances. With the distance from the dust source,
365 supermicron particles will settle, and submicron particles may then dominate ice nucleation on the global scale. Therefore,
366 including the particle size class in INP parameterizations can improve predictions of ice formation in clouds. The
367 overprediction of AMD freezing ability demonstrated in this study, by the Atkinson et al. (2013) and Ullrich et al. (2017)
368 parameterizations, especially for submicron particles, emphasize the importance of future studies to better quantify the changes
369 in the ice-nucleating properties of AMD by atmospheric processing.
370
371

https://doi.org/10.5194/acp-2019-511
Preprint. Discussion started: 6 June 2019


Atmospheric Chemistry and Physics Discussions

372 **Data availability**. Data are available upon request to the first author.

373

374 **Author contributions.** NR and YR designed the experiments, carried out the field measurements, conducted freezing
375 experiments in WISDOM, and wrote the paper. CB, LE and TK designed and performed freezing experiments in BINARY.
376 SRR performed backtrajectory analyses. NR and IKA performed the chemical analyses of filters. All authors contributed to
377 the discussion and analysis of data and the writing of the manuscript.

378

379 **Competing interests.** The authors declare that they have no conflict of interest.

380 **Acknowledgments**

381 This study was partially funded by the Israel Science Foundation (grant #236/16). The authors are grateful for funding by the
382 German Research Foundation (DFG) through the research unit FOR 1525 (INUIT) under KO 2944/2-2 for C.B. and T.K., and
383 a Mercator Fellowship for Y.R., and acknowledge the support from The Helen Kimmel Center for Planetary Sciences, and the
384 de Botton Center for Marine Sciences. Analyses and visualizations of MERRA data in this study were produced with the
385 Giovanni online data system, developed and maintained by the NASA GES DISC (http://giovanni.sci.gsfc.nasa.gov/Giovanni),
386 PM_{10} data is available from the Israel Ministry of Environmental Protection website
387 (http://www.svivaaqm.net/Default.rtl.aspx). Other data used in this study can be retrieved from osf.io/gpuqt.

388 **References**

389 Ansmann, A., Tesche, M., Althausen, D., Müller, D., Seifert, P., Freudenthaler, V., Heese, B., Wiegner, M., Pisani, G.,
390 Knippertz, P., and Dubovik, O.: Influence of Saharan dust on cloud glaciation in southern Morocco during the Saharan
391 Mineral Dust Experiment, Journal of Geophysical Research: Atmospheres, 113, D04210, 2008.
392 Atkinson, J. D., Murray, B. J., Woodhouse, M. T., Whale, T. F., Baustian, K. J., Carslaw, K. S., Dobbie, S., O/'Sullivan, D.,
393 and Malkin, T. L.: The importance of feldspar for ice nucleation by mineral dust in mixed-phase clouds, Nature, 498, 355-
394 358, 2013.
395 Augustin-Bauditz, S., Wex, H., Kanter, S., Ebert, M., Niedermeier, D., Stolz, F., Prager, A., and Stratmann, F.: The
396 immersion mode ice nucleation behavior of mineral dusts: A comparison of different pure and surface modified dusts,
397 Geophysical Research Letters, 41, 7375-7382, 2014.
398 Ben-Ami, Y., Koren, I., Rudich, Y., Artaxo, P., Martin, S. T., and Andreae, M. O.: Transport of North African dust from the
399 Bodélé depression to the Amazon Basin: a case study, Atmos. Chem. Phys., 10, 7533-7544, 2010.
400 Boose, Y., Sierau, B., García, M. I., Rodríguez, S., Alastuey, A., Linke, C., Schnaiter, M., Kupiszewski, P., Kanji, Z. A., and
401 Lohmann, U.: Ice nucleating particles in the Saharan Air Layer, Atmospheric Chemistry and Physics, 16, 9067-9087, 2016a.
402 Boose, Y., Welti, A., Atkinson, J., Ramelli, F., Danielczok, A., Bingemer, H. G., Plötze, M., Sierau, B., Kanji, Z. A., and
403 Lohmann, U.: Heterogeneous ice nucleation on dust particles sourced from 9 deserts worldwide–Part 1: Immersion freezing,
404 Atmos. Chem. Phys. , 2016b. 15075-15095, 2016b.
405 Broadley, S. L., Murray, B. J., Herbert, R. J., Atkinson, J. D., Dobbie, S., Malkin, T. L., Condliffe, E., and Neve, L.:
406 Immersion mode heterogeneous ice nucleation by an illite rich powder representative of atmospheric mineral dust, Atmos.
407 Chem. Phys., 12, 287-307, 2012.

https://doi.org/10.5194/acp-2019-511
Preprint. Discussion started: 6 June 2019

Atmospheric Chemistry and Physics Discussions

Budke, C. and Koop, T.: BINARY: an optical freezing array for assessing temperature and time dependence of heterogeneous ice nucleation, Atmos. Meas. Tech., 8, 689-703, 2015.
Cantrell, W. and Heymsfield, A.: Production of Ice in Tropospheric Clouds: A Review, Bulletin of the American Meteorological Society, 86, 795-807, 2005.
Chakrabarty, R. K., Beres, N. D., Moosmüller, H., China, S., Mazzoleni, C., Dubey, M. K., Liu, L., and Mishchenko, M. I.: Soot superaggregates from flaming wildfires and their direct radiative forcing, Scientific reports, 4, 5508, 2014.
Chiapello, I., Bergametti, G., Chatenet, B., Dulac, F., Jankowiak, I., Liousse, C., and Soares, E. S.: Contribution of the different aerosol species to the aerosol mass load and optical depth over the northeastern tropical Atlantic, Journal of Geophysical Research: Atmospheres, 104, 4025-4035, 1999.
Claquin, T., Schulz, M., and Balkanski, Y.: Modeling the mineralogy of atmospheric dust sources, Journal of Geophysical Research: Atmospheres, 104, 22243-22256, 1999.
Cziczo, D. J. and Froyd, K. D.: Sampling the composition of cirrus ice residuals, Atmospheric research, 142, 15-31, 2014.
Cziczo, D. J., Garimella, S., Raddatz, M., Hoehler, K., Schnaiter, M., Saathoff, H., Moehler, O., Abbatt, J. P., and Ladino, L. A.: Ice nucleation by surrogates of Martian mineral dust: What can we learn about Mars without leaving Earth?, Journal of Geophysical Research: Planets, 118, 1945-1954, 2013.
Dayan, U.: Climatology of Back Trajectories from Israel Based on Synoptic Analysis, Journal of Climate and Applied Meteorology, 25, 591-595, 1986.
Dee, D. P., Uppala, S., Simmons, A., Berrisford, P., Poli, P., Kobayashi, S., Andrae, U., Balmaseda, M., Balsamo, G., and Bauer, d. P.: The ERA-Interim reanalysis: Configuration and performance of the data assimilation system, Quarterly Journal of the royal meteorological society, 137, 553-597, 2011.
DeMott, P. J., Prenni, A. J., Liu, X., Kreidenweis, S. M., Petters, M. D., Twohy, C. H., Richardson, M. S., Eidhammer, T., and Rogers, D. C.: Predicting global atmospheric ice nuclei distributions and their impacts on climate, Proceedings of the National Academy of Sciences, 107, 11217-11222, 2010.
DeMott, P. J., Sassen, K., Poellot, M. R., Baumgardner, D., Rogers, D. C., Brooks, S. D., Prenni, A. J., and Kreidenweis, S. M.: African dust aerosols as atmospheric ice nuclei, Geophysical Research Letters, 30, n/a-n/a, 2003.
Engelbrecht, J. P., McDonald, E. V., Gillies, J. A., "Jay" Jayanty, R., Casuccio, G., and Gertler, A. W.: Characterizing mineral dusts and other aerosols from the Middle East—Part 2: Grab samples and re-suspensions, Inhalation toxicology, 21, 327-336, 2009.
Ganor, Foner, H. A., Brenner, S., Neeman, E., and Lavi, N.: The chemical composition of aerosols settling in Israel following dust storms, Atmospheric Environment. Part A. General Topics, 25, 2665-2670, 1991.
Ganor, E., Osetinsky, I., Stupp, A., and Alpert, P.: Increasing trend of African dust, over 49 years, in the eastern Mediterranean, Journal of Geophysical Research: Atmospheres, 115, D07201, 2010.
Garrison, V. H., Shinn, E. A., Foreman, W. T., Griffin, D. W., Holmes, C. W., Kellogg, C. A., Majewski, M. S., Richardson, L. L., Ritchie, K. B., and Smith, G. W.: African and Asian Dust: From Desert Soils to Coral Reefs, BioScience, 53, 469-480, 2003.
Gat, D., Mazar, Y., Cytryn, E., and Rudich, Y.: Origin-Dependent Variations in the Atmospheric Microbiome Community in Eastern Mediterranean Dust Storms, Environmental Science & Technology, 51, 6709-6718, 2017.
Gelaro, R., McCarty, W., Suárez, M. J., Todling, R., Molod, A., Takacs, L., Randles, C. A., Darmenov, A., Bosilovich, M. G., and Reichle, R.: The modern-era retrospective analysis for research and applications, version 2 (MERRA-2), Journal of Climate, 30, 5419-5454, 2017.
Hader, J. D., Wright, T. P., and Petters, M. D.: Contribution of pollen to atmospheric ice nuclei concentrations, Atmos. Chem. Phys., 14, 5433-5449, 2014.
Hiranuma, N., Augustin-Bauditz, S., Bingemer, H., Budke, C., Curtius, J., Danielczok, A., Diehl, K., Dreischmeier, K., Ebert, M., Frank, F., Hoffmann, N., Kandler, K., Kiselev, A., Koop, T., Leisner, T., Möhler, O., Nillius, B., Peckhaus, A., Rose, D., Weinbruch, S., Wex, H., Boose, Y., DeMott, P. J., Hader, J. D., Hill, T. C. J., Kanji, Z. A., Kulkarni, G., Levin, E. J. T., McCluskey, C. S., Murakami, M., Murray, B. J., Niedermeier, D., Petters, M. D., O'Sullivan, D., Saito, A., Schill, G. P., Tajiri, T., Tolbert, M. A., Welti, A., Whale, T. F., Wright, T. P., and Yamashita, K.: A comprehensive laboratory study on the immersion freezing behavior of illite NX particles: a comparison of 17 ice nucleation measurement techniques, Atmos. Chem. Phys., 15, 2489-2518, 2015.

https://doi.org/10.5194/acp-2019-511
Preprint. Discussion started: 6 June 2019


Atmospheric Chemistry and Physics Discussions

Hoose, C., Lohmann, U., Erdin, R., and Tegen, I.: The global influence of dust mineralogical composition on heterogeneous ice nucleation in mixed-phase clouds, Environmental Research Letters, 3, 025003, 2008.
Hoose, C. and Möhler, O.: Heterogeneous ice nucleation on atmospheric aerosols: a review of results from laboratory experiments, Atmos. Chem. Phys., 12, 9817-9854, 2012.
Huffman, J. A., Prenni, A. J., DeMott, P. J., Pöhlker, C., Mason, R. H., Robinson, N. H., Fröhlich-Nowoisky, J., Tobo, Y., Després, V. R., Garcia, E., Gochis, D. J., Harris, E., Müller-Germann, I., Ruzene, C., Schmer, B., Sinha, B., Day, D. A., Andreae, M. O., Jimenez, J. L., Gallagher, M., Kreidenweis, S. M., Bertram, A. K., and Pöschl, U.: High concentrations of biological aerosol particles and ice nuclei during and after rain, Atmos. Chem. Phys., 13, 6151-6164, 2013.
IPCC: IPCC: Climate Change 2013, The Physical Science Basis, Cambridge University Press, Cambridge, United Kingdom and New York, NY, USA., 2013. 2013.
Jickells, T. D., An, Z. S., Andersen, K. K., Baker, A. R., Bergametti, G., Brooks, N., Cao, J. J., Boyd, P. W., Duce, R. A., Hunter, K. A., Kawahata, H., Kubilay, N., laRoche, J., Liss, P. S., Mahowald, N., Prospero, J. M., Ridgwell, A. J., Tegen, I., and Torres, R.: Global Iron Connections Between Desert Dust, Ocean Biogeochemistry, and Climate, Science, 308, 67-71, 2005.
Kalderon-Asael, B., Erel, Y., Sandler, A., and Dayan, U.: Mineralogical and chemical characterization of suspended atmospheric particles over the east Mediterranean based on synoptic-scale circulation patterns, Atmospheric Environment, 43, 3963-3970, 2009.
Kandler, K., Benker, N., Bundke, U., Cuevas, E., Ebert, M., Knippertz, P., Rodríguez, S., Schütz, L., and Weinbruch, S.: Chemical composition and complex refractive index of Saharan Mineral Dust at Izana, Tenerife (Spain) derived by electron microscopy, Atmospheric Environment, 41, 8058-8074, 2007.
Kanji, Z. A., Ladino, L. A., Wex, H., Boose, Y., Burkert-Kohn, M., Cziczo, D. J., and Krämer, M.: Overview of ice nucleating particles, Meteor. Mon, 58, 1.1-1.33, 2017.
Kaufmann, L., Marcolli, C., Hofer, J., Pinti, V., Hoyle, C. R., and Peter, T.: Ice nucleation efficiency of natural dust samples in the immersion mode, Atmos. Chem. Phys., 16, 11177-11206, 2016.
Khvorostyanov, V. I. and Curry, J. A.: The theory of ice nucleation by heterogeneous freezing of deliquescent mixed CCN. Part I: Critical radius, energy, and nucleation rate, Journal of the atmospheric sciences, 61, 2676-2691, 2004.
Koop, T. and Murray, B. J.: A physically constrained classical description of the homogeneous nucleation of ice in water, The Journal of Chemical Physics, 145, 211915, 2016.
Koren, I., Yoram, J. K., Richard, W., Martin, C. T., Yinon, R., Martins, J. V., and Daniel, R.: The Bodélé depression: a single spot in the Sahara that provides most of the mineral dust to the Amazon forest, Environmental Research Letters, 1, 014005, 2006.
Krasnov, H., Katra, I., Koutrakis, P., and Friger, M. D.: Contribution of dust storms to PM10 levels in an urban arid environment, Journal of the Air & Waste Management Association, 64, 89-94, 2014.
Laskin, A., Iedema, M. J., Ichkovich, A., Graber, E. R., Taraniuk, I., and Rudich, Y.: Direct observation of completely processed calcium carbonate dust particles, Faraday Discussions, 130, 453-468, 2005.
Levin, Z., Ganor, E., and Gladstein, V.: The effects of desert particles coated with sulfate on rain formation in the eastern Mediterranean, Journal of Applied Meteorology, 35, 1511-1523, 1996.
Mahowald, N., Albani, S., Kok, J. F., Engelstaeder, S., Scanza, R., Ward, D. S., and Flanner, M. G.: The size distribution of desert dust aerosols and its impact on the Earth system, Aeolian Research, 15, 53-71, 2014.
Marcolli, C., Gedamke, S., Peter, T., and Zobrist, B.: Efficiency of immersion mode ice nucleation on surrogates of mineral dust, Atmos. Chem. Phys., 7, 5081-5091, 2007.
Marple, V. A., Rubow, K. L., and Behm, S. M.: A Microorifice Uniform Deposit Impactor (MOUDI): Description, Calibration, and Use, Aerosol Science and Technology, 14, 434-446, 1991.
Mason, R. H., Chou, C., McCluskey, C. S., Levin, E. J. T., Schiller, C. L., Hill, T. C. J., Huffman, J. A., DeMott, P. J., and Bertram, A. K.: The micro-orifice uniform deposit impactor–droplet freezing technique (MOUDI-DFT) for measuring concentrations of ice nucleating particles as a function of size: improvements and initial validation, Atmos. Meas. Tech., 8, 2449-2462, 2015.
Mazar, Y., Cytryn, E., Erel, Y., and Rudich, Y.: Effect of dust storms on the atmospheric microbiome in the Eastern Mediterranean, Environmental science & technology, 50, 4194-4202, 2016.
Middleton, N.: Desert dust hazards: A global review, Aeolian research, 24, 53-63, 2017.

https://doi.org/10.5194/acp-2019-511
Preprint. Discussion started: 6 June 2019

Atmospheric Chemistry and Physics Discussions

507 Middleton, N. J. and Goudie, A. S.: Saharan dust: sources and trajectories, Transactions of the Institute of British
508 Geographers, 26, 165-181, 2001.
509 Möhler, O., Benz, S., Saathoff, H., Schnaiter, M., Wagner, R., Schneider, J., Walter, S., Ebert, V., and Wagner, S.: The
510 effect of organic coating on the heterogeneous ice nucleation efficiency of mineral dust aerosols, Environmental Research
511 Letters, 3, 025007, 2008.
512 Murray, B. J., O'Sullivan, D., Atkinson, J. D., and Webb, M. E.: Ice nucleation by particles immersed in supercooled cloud
513 droplets, Chemical Society Reviews, 41, 6519-6554, 2012.
514 Niedermeier, D., Augustin-Bauditz, S., Hartmann, S., Wex, H., Ignatius, K., and Stratmann, F.: Can we define an asymptotic
515 value for the ice active surface site density for heterogeneous ice nucleation?, Journal of Geophysical Research:
516 Atmospheres, 120, 5036-5046, 2015.
517 Niemand, M., Möhler, O., Vogel, B., Vogel, H., Hoose, C., Connolly, P., Klein, H., Bingemer, H., DeMott, P., Skrotzki, J.,
518 and Leisner, T.: A Particle-Surface-Area-Based Parameterization of Immersion Freezing on Desert Dust Particles, Journal of
519 the Atmospheric Sciences, 69, 3077-3092, 2012.
520 Perlwitz, J., Pérez García-Pando, C., and Miller, R.: Predicting the mineral composition of dust aerosols–Part 1:
521 Representing key processes, Atmospheric Chemistry and Physics, 15, 11593-11627, 2015.
522 Price, H., Baustian, K., McQuaid, J., Blyth, A., Bower, K., Choularton, T., Cotton, R., Cui, Z., Field, P., and Gallagher, M.:
523 Atmospheric Ice-Nucleating Particles in the Dusty Tropical Atlantic, Journal of Geophysical Research: Atmospheres, 123,
524 2175-2193, 2018.
525 Prospero, J. M.: Long-range transport of mineral dust in the global atmosphere: Impact of African dust on the environment
526 of the southeastern United States, Proceedings of the National Academy of Sciences, 96, 3396-3403, 1999.
527 Pruppacher, H. and Klett, J.: Microphysics of Clouds and Precipitation: With an Introduction to Cloud Chemistry and Cloud
528 Electricity, 954 pp. Springer, New York, 1997.
529 Reicher, N., Segev, L., and Rudich, Y.: The WeIzmann Supercooled Droplets Observation on a Microarray (WISDOM) and
530 application for ambient dust, Atmospheric Measurement Techniques, 11, 233, 2018.
531 Rosenfeld, D., Rudich, Y., and Lahav, R.: Desert dust suppressing precipitation: a possible desertification feedback loop, P.
532 Natl. Acad. Sci., 98, 5975–5980. 2001.
533 Rosenfeld, D. and Woodley, W. L.: Deep convective clouds with sustained supercooled liquid water down to -
534 37.5[thinsp][deg]C, Nature, 405, 440-442, 2000.
535 Sprenger, M. and Wernli, H.: The LAGRANTO Lagrangian analysis tool–version 2.0, Geoscientific Model Development, 8,
536 2569, 2015.
537 Sullivan, R. C., Petters, M. D., DeMott, P. J., Kreidenweis, S. M., Wex, H., Niedermeier, D., Hartmann, S., Clauss, T.,
538 Stratmann, F., and Reitz, P.: Irreversible loss of ice nucleation active sites in mineral dust particles caused by sulphuric acid
539 condensation, Atmospheric Chemistry and Physics, 10, 11471-11487, 2010.
540 Tegen, I. and Fung, I.: Modeling of mineral dust in the atmosphere: Sources, transport, and optical thickness, Journal of
541 Geophysical Research: Atmospheres, 99, 22897-22914, 1994.
542 Twohy, C. and Poellot, M.: Chemical characteristics of ice residual nuclei in anvil cirrus clouds: evidence for homogeneous
543 and heterogeneous ice formation, Atmospheric Chemistry and Physics, 5, 2289-2297, 2005.
544 Ullrich, R., Hoose, C., Möhler, O., Niemand, M., Wagner, R., Höhler, K., Hiranuma, N., Saathoff, H., and Leisner, T.: A
545 New Ice Nucleation Active Site Parameterization for Desert Dust and Soot, Journal of the Atmospheric Sciences, 74, 699-
546 717, 2017.
547 Vali, G.: Quantitative Evaluation of Experimental Results an the Heterogeneous Freezing Nucleation of Supercooled
548 Liquids, Journal of the Atmospheric Sciences, 28, 402-409, 1971.
549 Zimmermann, F., Weinbruch, S., Schütz, L., Hofmann, H., Ebert, M., Kandler, K., and Worringen, A.: Ice nucleation
550 properties of the most abundant mineral dust phases, Journal of Geophysical Research: Atmospheres, 113, 2008.
551

552

553

554

https://doi.org/10.5194/acp-2019-511
Preprint. Discussion started: 6 June 2019

Atmospheric Chemistry and Physics Discussions

555

556 **Table 1: Summary of the investigated dust storm events. The events are denoted by their geographic origin: Saharan dust storms**
557 **(SDS), Syrian dust storm (SyDS), mixed contribution of the two (MDS), and mix of dust event with a free-dust period (CSDS).**

Event	Start [UTC]	Sampling period [hour]	PM10 peak [μg m^{-3}]	PM10 mean [μg m^{-3}]	Freezing analysis technique
SyDS1 19 April 2016	07:30	25	132	76±20	WISDOM
CSDS 27 April 2016	07:30	24	67	30±13	WISDOM, BINARY
SyDS2 23 November 2016	15:30	18	332	184±68	WISDOM
SDS1 09 March 2017	11:00	48	387	96±66	WISDOM
SDS2 12 March 2017	12:00	24	717	206±120	WISDOM
MDS 12 April 2017	13:30	25	409	141±106	WISDOM

558

559

560

561

562

https://doi.org/10.5194/acp-2019-511
Preprint. Discussion started: 6 June 2019

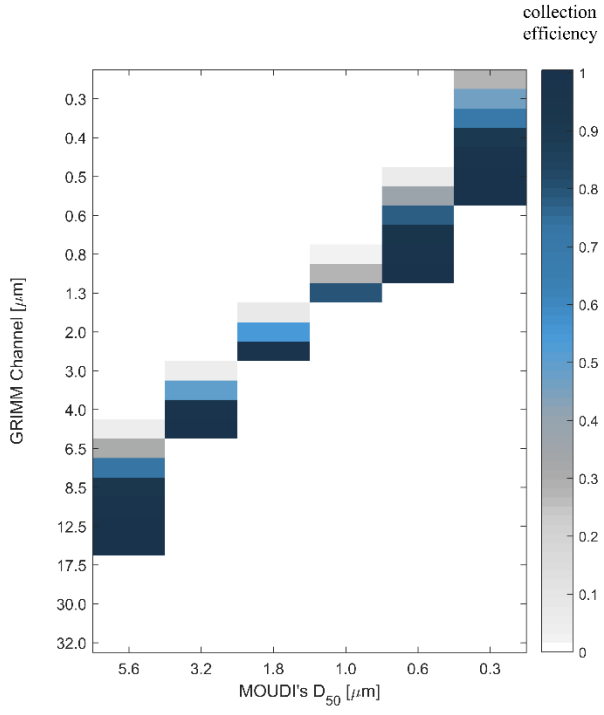

Figure 1: A conversion matrix of GRIMM channels to MOUDI stages. The conversion was based on collection efficiency curves from Marple et al. (1991). The color shades represent the fraction of particles of a specific GRIMM channel to be impacted on a specific MOUDI stage.

https://doi.org/10.5194/acp-2019-511
Preprint. Discussion started: 6 June 2019

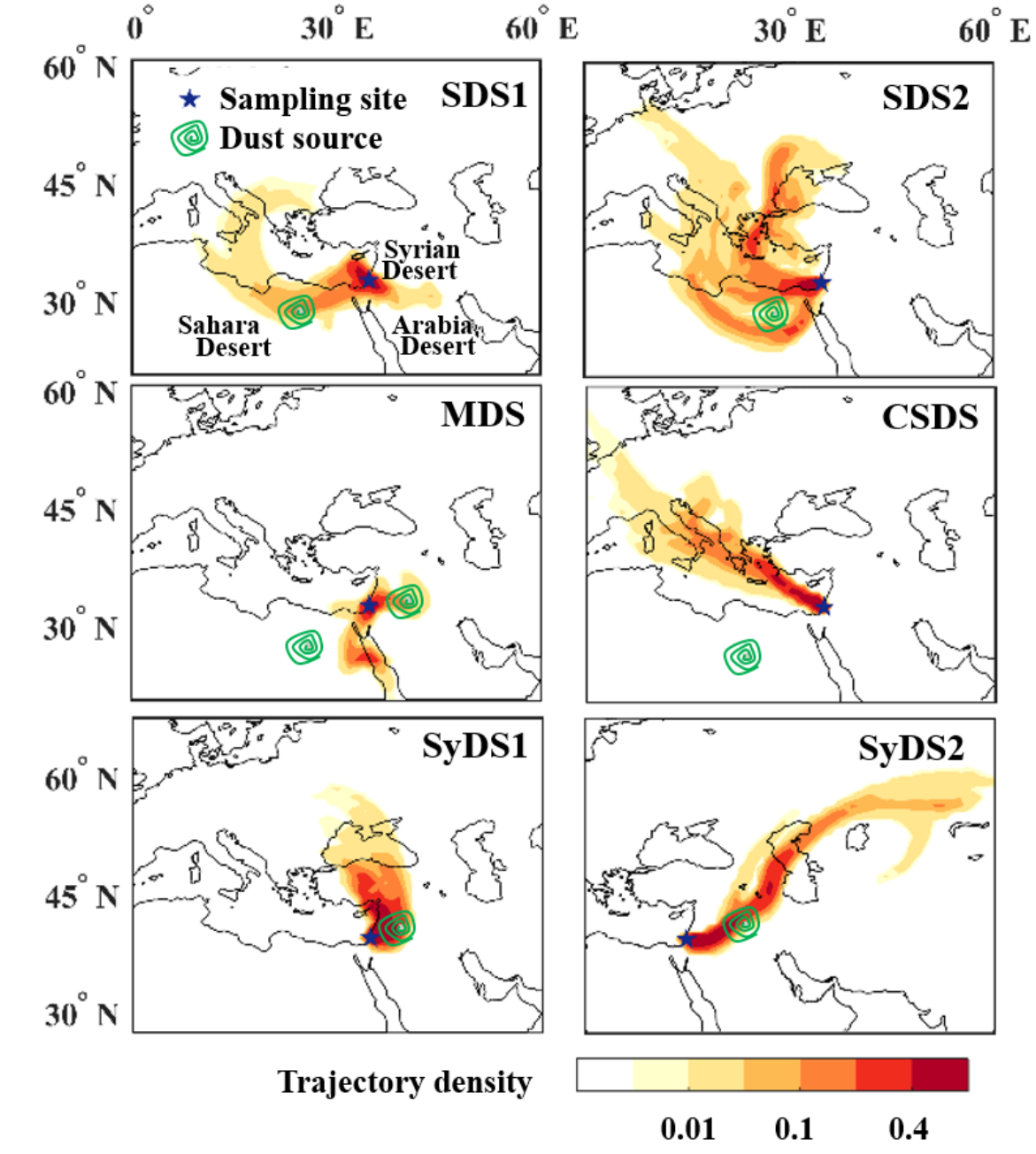

Figure 2: Air mass origin and atmospheric paths of the dust events. Colors represent the density of 72-h backward air mass trajectories (normalized to the total trajectory counts). The green contours represent the geographic locations where a high mass of the dust occurred during the air mass transition, which defined as the potential origin of the dust. Abbreviations in the top right of each panel indicate the particular dust event.

https://doi.org/10.5194/acp-2019-511
Preprint. Discussion started: 6 June 2019

Atmospheric Chemistry and Physics Discussions

573

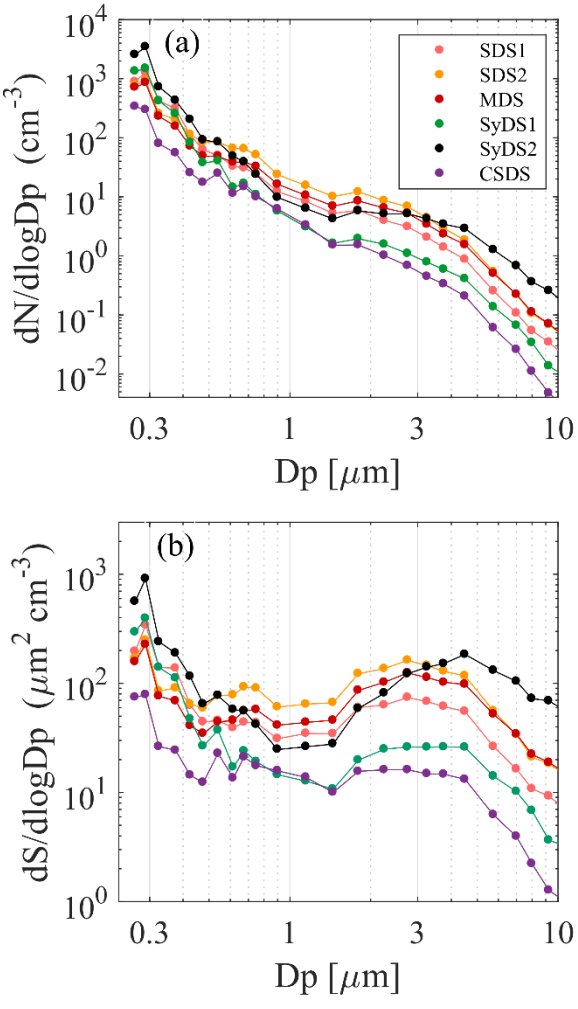

574

575 **Figure 3: Particle size distributions. Particle number size (a) and surface area size (b) distributions averaged over the entire sampling**
576 **periods as monitored by GRIMM OPC during the studied events. Dp is the diameter of the particles and set at the center of each**
577 **GRIMM channel.**

578

https://doi.org/10.5194/acp-2019-511
Preprint. Discussion started: 6 June 2019

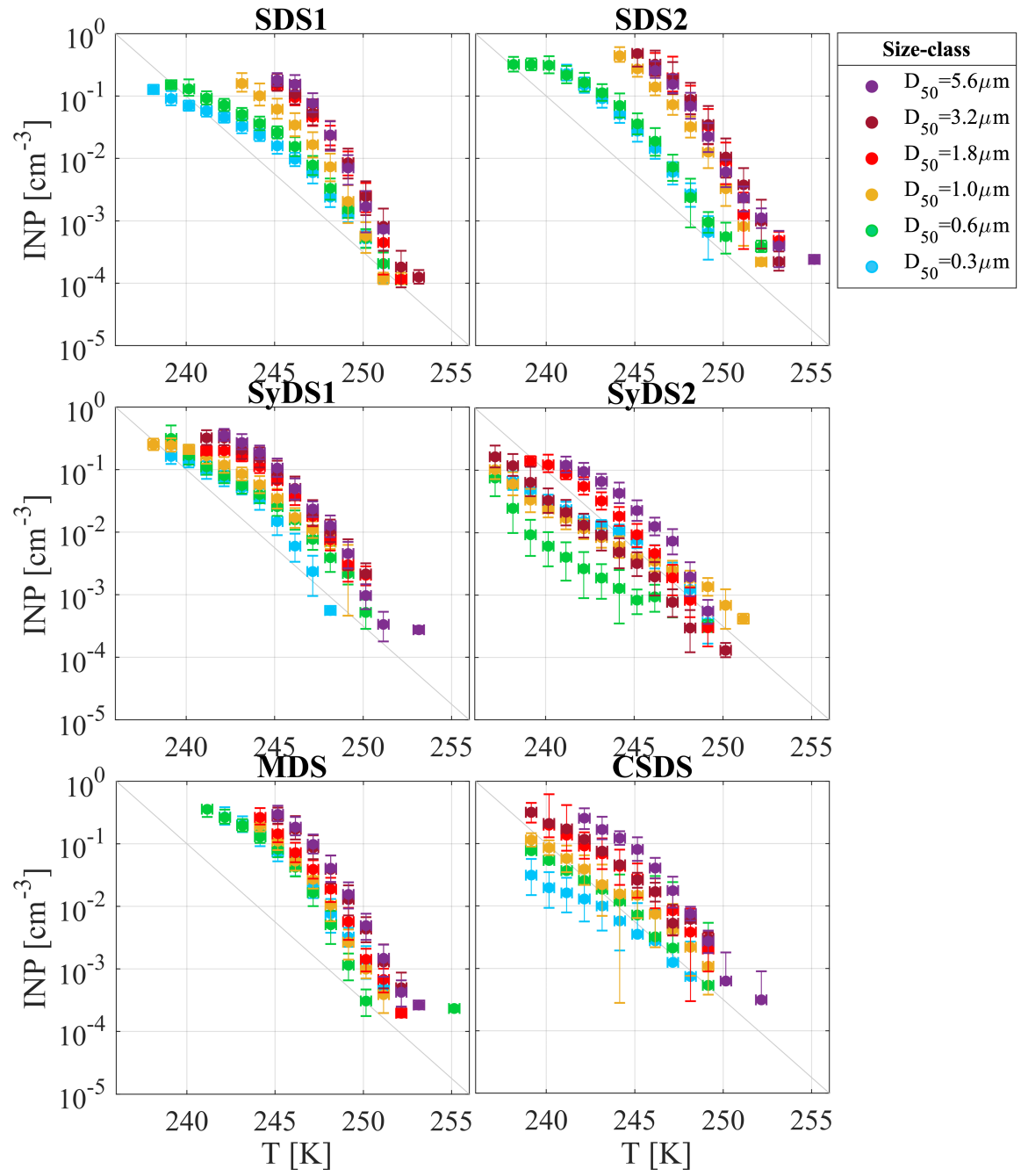

Figure 4: Airborne INP concentrations measured during dust events. INP concentrations per cm^{-3} air as function of temperature, presented in different colors for the different particle size-classes. Uncertainty in temperature is 0.3 K. The grey diagonal line is presented for orientation only.

https://doi.org/10.5194/acp-2019-511
Preprint. Discussion started: 6 June 2019

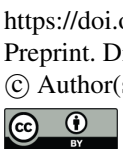

Atmospheric Chemistry and Physics Discussions

585

586

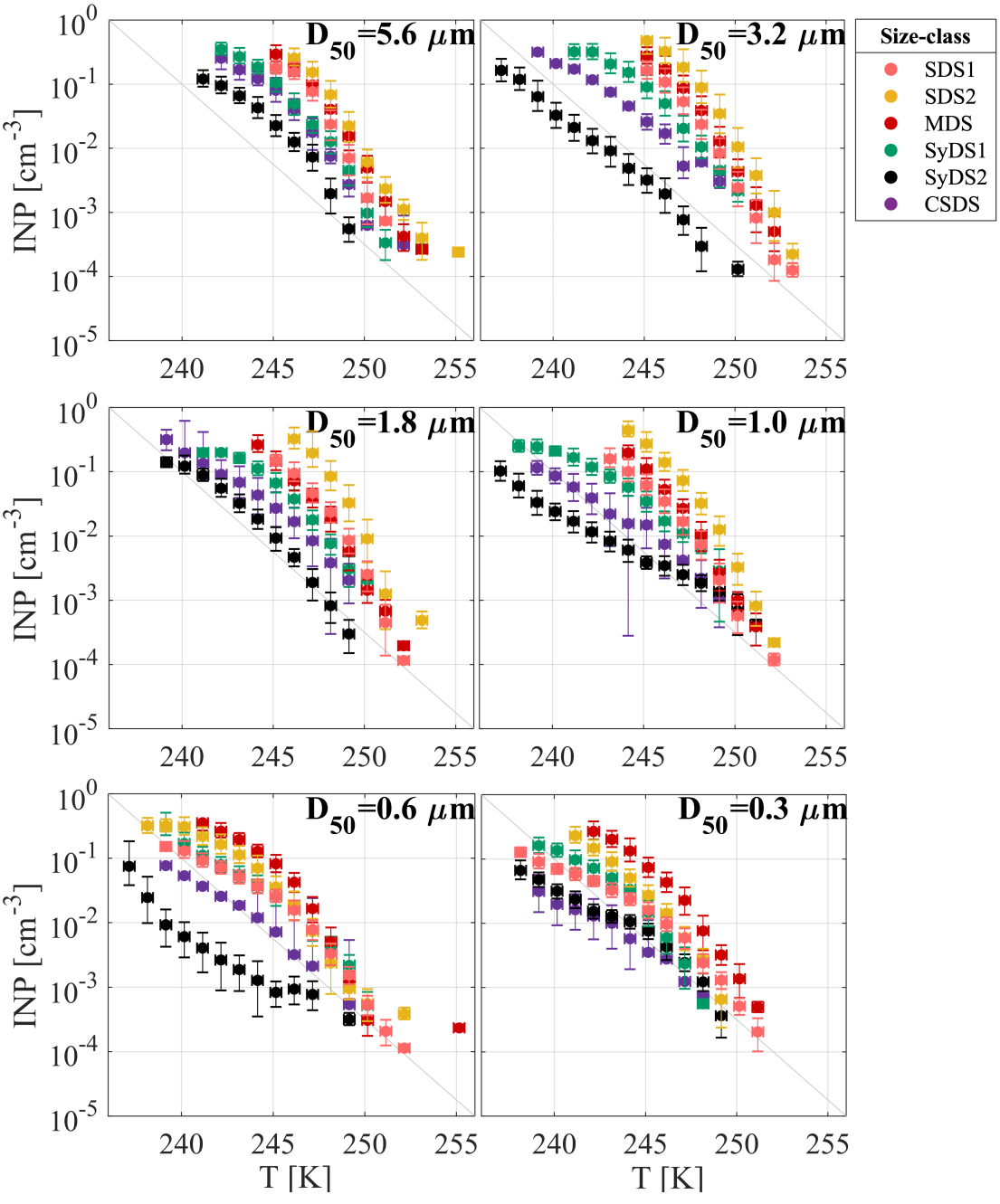

587

588 **Figure 5: Airborne INP concentrations for various size classes. INP concentrations per cm^{-3} air as function of temperature, presented**
589 **in different colors for the different dust events that were sampled. Uncertainty in temperature is 0.3 K. The grey diagonal line is**
590 **presented for orientation only.**

https://doi.org/10.5194/acp-2019-511
Preprint. Discussion started: 6 June 2019

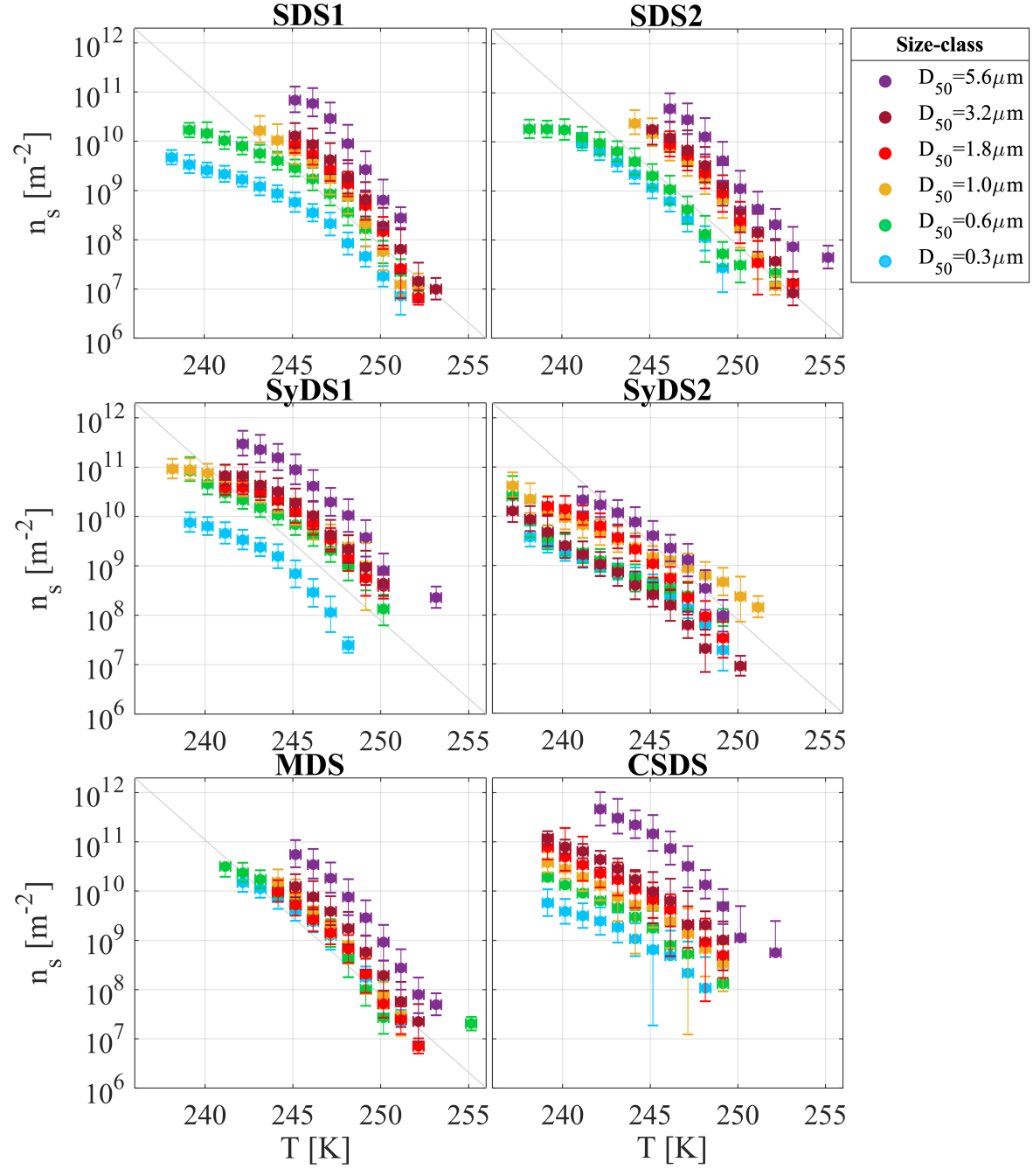

Figure 6: Ice active site density as a function of temperature, $n_s(T)$, for airborne particles dominated by mineral dust are presented individually for each dust event. The different colors represent the different size-classes that were investigated. SDS, SyDS and MDS represent Saharan, Syrian, and mixed dust events, respectively (see text for more details). The linear grey line is identical in each panel to facilitate comparison.

https://doi.org/10.5194/acp-2019-511
Preprint. Discussion started: 6 June 2019

Atmospheric Chemistry and Physics Discussions

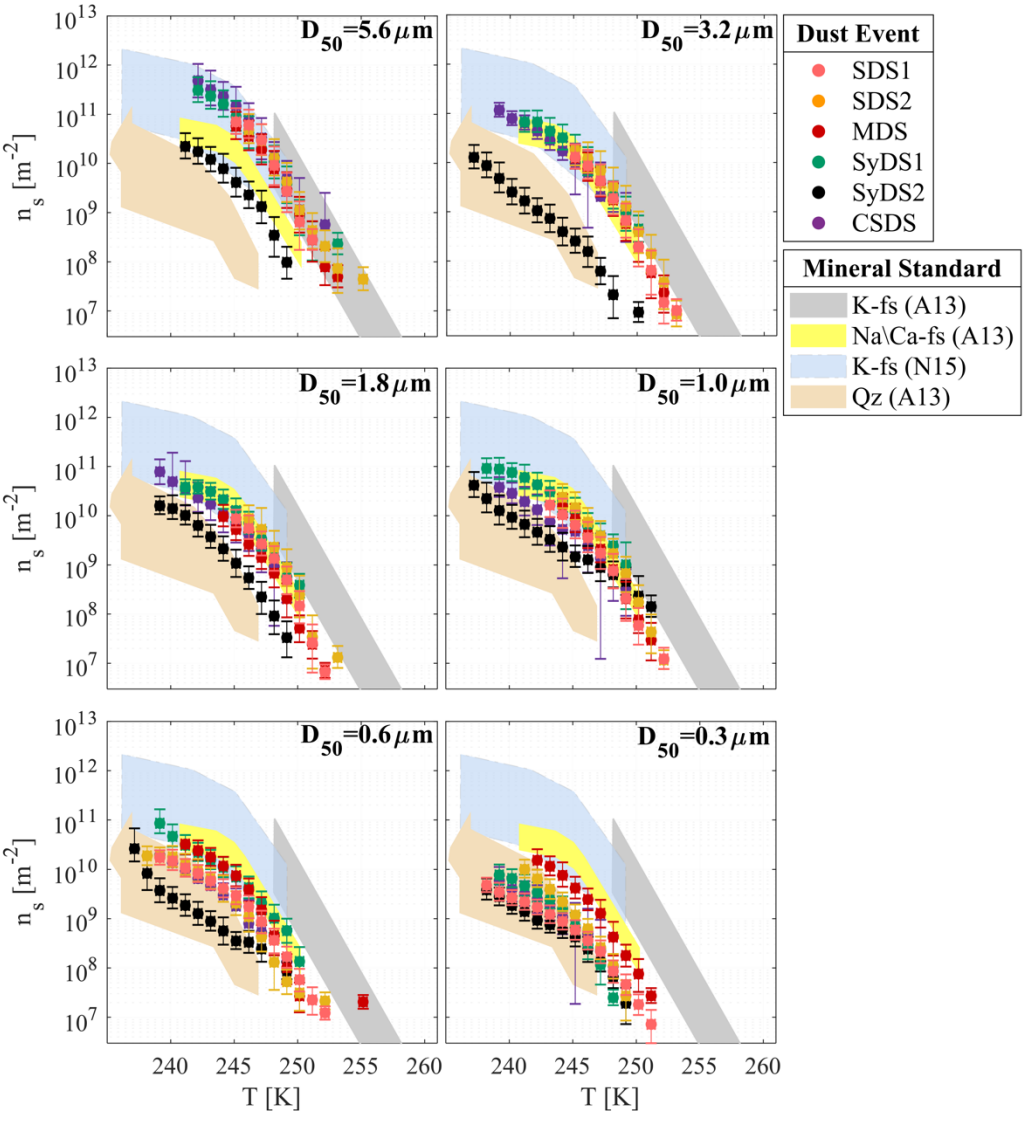

Figure 7: Ice active site density during dust events in different particle size classes. Dust events from the Sahara Desert (SDS), Syrian Desert (SyDS), or both (MDS) are marked by the different colors. Data for D_{50} = 3.2, 1.8 and 1.0 µm of SDS#2 adopted from Reicher et al. (2018). Relevant standard minerals scaled to ambient values are shown: K-feldspar (K-fs), Na\Ca-feldspar (Na\Ca-fs) and quartz (Qz) from Atkinson et al. (2013), and K-fs from Niedermeier et al. (2015).

https://doi.org/10.5194/acp-2019-511
Preprint. Discussion started: 6 June 2019

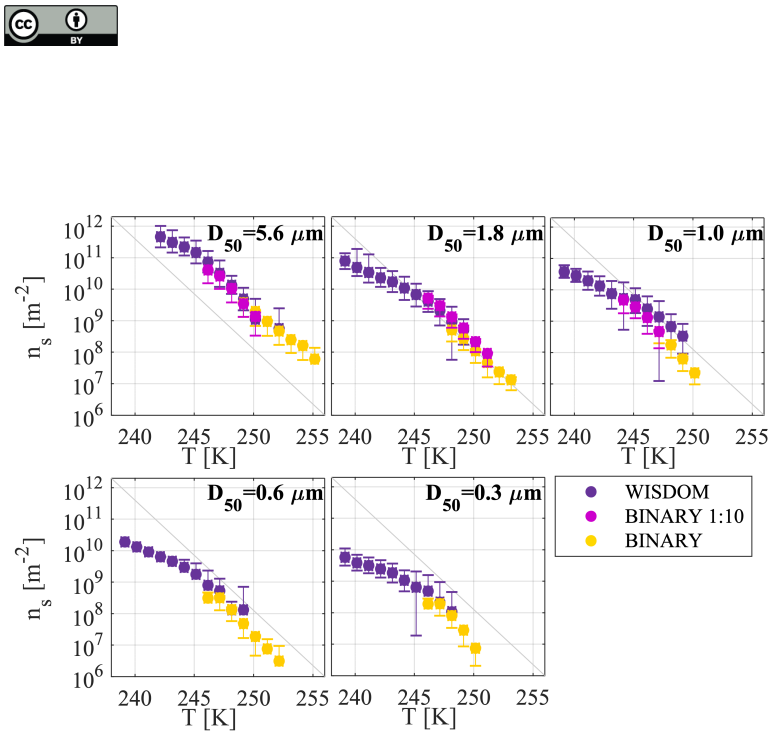

606

607 **Figure 8: Complementary measurements of WISDOM and BINARY for CSDS. Analysis in the BINARY was performed to increased**
608 **detection sensitivity of ice active site densities. Two suspension with different dilution factors were analysed by BINARY and are**
609 **compared here to the WISDOM data for the different size-classes.**

610

611

612

613

614

615

616

https://doi.org/10.5194/acp-2019-511
Preprint. Discussion started: 6 June 2019

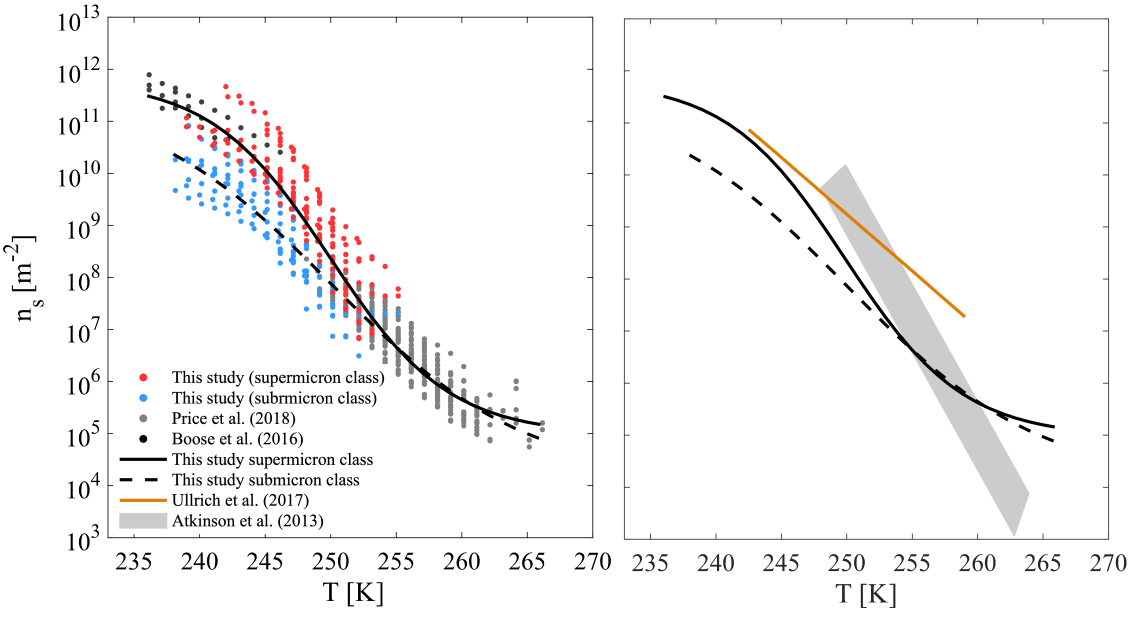

Figure 9: Heterogeneous ice nucleation by airborne particles during dusty conditions. (a) Active site densities of supermicron and submicron size-classes from this study are shown together with flight data (Price et al. (2018)) and deposited or *in-situ* data (Boose et al. (2016b)). New parameterizations, which were derived in this work based on the combined AMD data of the different studies, are shown for supermicron and submicron classes. (b) The new parameterizations derived in this study based on all AMD data, shown next to recent parameterizations for desert dust by Ullrich et al. (2017) and K-feldspar predictions by Atkinson et al. (2013).